Eighteenth Indian Expeditin to Antarctica, Scientific Report, 2002
Department of Ocean Development. Technical Publication No. 16 pp 153-190

A COMPARITIVE STUDY OF GLACIO-METEOROLOGICAL PARAMETERS, REFLECTANCE AND SURFACE ENERGY EXCHANGE OVER DIFFERENT SNOW-ICE MEDIA IN DRONNING MAUD LAND IN EAST ANATRCTICA

Praveen Kumar Srivastava
Snow and Avalanche Study Establishment, Manali

Abstract

Two Automatic Weather Stations (AWS) were installed over continental shelf and continental ice surfaces in Dronning Maud Land in East Antarctica during XVIIth Indian Scientific Expedition to Antarctica (ISEA). High quality glacio-meteorological data were collected round the year. A simple energy balance model based on the glacio-met parameters is formulated to calculate the energy exchange over the two types of surfaces. Surface roughness and albedo values of the two types of surfaces have been accounted for in the model. Different components of energy budget are tabulated and the results are compared for the two types of surfaces during Austral summer of 1999-2000. Summer and winter energy budget are also compared and discussed for the continental ice surface. The difference in the energy balance over continental shelf and continental ice is mainly caused by differences in albedo, surface roughness and short-wave extinction coefficient. The average energy budget over continental ice was found to be negative during both summer and winter period. Results indicate that the main difference in summer and winter energy budget over continental ice is in the net radiation and sensitive heat fluxes during the corresponding periods. As the energy balance models are sensitive to surface reflectivity variation, albedo measurements over different snow-ice media were carried out and its dependence on solar elevation angle and cloud amount/type were investigated in detail.

The albedo of sea-ice in the southern ocean was also investigated during the sea voyage to Antarctica. The mean albedo varied from 12 % for open water to 61 % for 10/10 sea-ice concentration with average value of 43 % for the observational period. The measured values are in agreement with those reported previously.

INTRODUCTION

To the human eye, the vast Antarctic ice sheet gives the impression of homo-geneity. However, large seasonal fluctuations in surface climate at these high latitudes

create substantial changes in surface energy balance. Long term fluctuations in the energy balance of Antarctic ice sheet are of considerable interest because of significant contribution to mass balance and its fluctuations resulting from green house induced warming, sublimation and melting. Energy balance investigations include knowledge of the structure of the atmosphere above the ice sheet as well as the physical processes at the surface and in snow and ice layers. Only with a thorough understanding of the atmospheric boundary layer and the energy- and mass- exchange processes can the response of the Antarctic ice sheet to changing climatic conditions be simulated by thermodynamic ice-sheet models (Huybrechts and others, 1991). The energy balance which includes net radiation, sensible heat flux, latent heat flux, latent heat of fusion and ground heat flux, determines the ablation process at the surface. These processes depend strongly on atmospheric conditions and surface properties. The problem thus involves quantifying the competing effects of energy balance components v/s net energy gain or loss over the surface. A major difficulty lies in the fact that due to sparse observatory network over the Antarctic continent, area averaged values for energy balance components in different snow-ice medium are still not precisely known or can at best be summed over as sketchy (Smith, 1998). Keeping this in view attention was focussed on studying the variation in snow-met parameters, radiative fluxes, short-wave reflectance (albedo) and surface energy balance over the Dronning Maud Land, East Antarctica. This paper examine and compares physical processes and the factors controlling energy balance over the continental shelf covered with thick layer of high density snow with that over the blue-ice (continental ice).

INSTRUMENTATION AND LOCATION OF MEASUREMENT SITES

In order to improve the data quality and to cover a large area with continuous radiation data, two Automatic Weather Stations (AWS) were installed during the austral summer of XVIIIth Indian Scientific Expedition to Antarctica. The AWS were set up at locations 70° 05' S, 12° E over continental shelf to study the radiative properties of snow & shelf ice and 70° 45' 52" S, 11^0 44' 3" E over the blue-ice. The location over the shelf is barely 18 km from the sea thus representing the coastal conditions. The site of the blue-ice station is very close to the grounding line, just behind the Schirmachar Oasis. The blue-ice site is of particular interest because though Antarctic blue-ice areas make up only a small part of the Antarctic continent, they are one of the few areas on the continent where ablation exceeds accumulation (Bintanja, 1995) i.e. surface energy balance is negative. The surface over the blue-ice is almost always free of snow while that on the shelf is always covered with snow with average density of 0.45 gm/cn^3 and depth of 1 to 1.5 meters. At both the locations, the surrounding topography is almost Hat and measurement sites are completely unshaded, so the affect of slope and aspect on the topoclimate are minimized.

The Sutron 8210 series data logger was used in the AWS, which has a wide range of inputs, designed to support the most common snow and met data collection applications. The system consists of Data Collection Platform (DCP) and various snow and meteorological sensors. The DCP acquires data after a predefined interval from different sensors. At the end of every hour this data is processed and stored locally. All the electronic components of the DCP are capable of operating up to -400C under extreme weather conditions. Salient features include:

- PCMCIA memory card slot for data or programming storage
- Dedicated external RS-232 serial port for programming and data retrieval
- Field programmable flash EPROM's via the use of PCMCIA port
- The AWS is equipped with the following sensors:
- Ambient temperature
- Relative humidity
- Wind direction and wind speed
- Atmospheric pressure
- Snow depth
- Albedometer (upward and downward looking pyranometers)
- Snow surface Temperature

Power is supplied by a solar panel combined with heavy-duty low temperature batteries. The entire assembly including the data logger, sensors, battery and solar panel are mounted on a triangular mast over the snow or ice surface.

THEORY OF RADIATIVE ENERGY EXCHANGE BETWEEN SNOW/ICE SURFACE AND ATMOSPHERE

If there is no horizontal transport of heat, conservation of energy requires that, at any point on the surface at any instant:

0)

where

B = net surface energy budget
S = net short-wave energy absorbed by surface
L = . net long-wave energy radiated/absorbed by the surface
H = sensible heat flux
LE= latent heat flux
Q_g = heat conduction at the glacier surface
Q_p = heat energy added to the surface due to precipitation

All these terms are measured/calculated in Wm^{-2} and positive for flux toward the surface, negative for fluxes away from the surface, For this study it is assumed that the last two terms are negligible components in daily energy balance of a surface when compared to the other terms. Therefore, neglecting those terms we get:

$$B = S + L + H + LE \quad (2)$$

The first two terms on the right hand side of the equation are net radiation budget components and the last two terms are the turbulent energy fluxes.

Short-wave radiation flux

The short-wave radiation reflected from the surface $S_{out}(\uparrow)$ depends on the amount of incident radiation $S_{in}(\downarrow)$ and the surface albedo a. The net short-wave radiation flux (S) absorbed by the surface is calculated as:

$$S = S_{in}(\downarrow)(1-a) \quad (3)$$

The temporal variation in albedo values is taken into account by tracking the hourly short wave reflected radiation from the surface.

Long-wave radiation Mux

Net long-wave radiation is the difference between incoming radiation from the atmosphere and emitted radiation from the snow surface. The snow-surface is considered almost a black body, as Dozier and Warren (1982) have noted, "in the infrared wavelengths, snow is one of the blackest substances on earth". Thus, outgoing longwave radiation, L_{out}, can be calculated using the Stefan-Boltzman law:

$$L_{out} = \varepsilon_s \sigma T s 4$$

where ε_s is the emissivity of the snow/ice surface with a value close to one; σ is the Stefan-Boltzman constant and T_s is the surface temperature.

Incoming long-wave radiation will depend on the temperature and composition of the overlying atmosphere and is calculated following a model developed by Prata (1996). This model computes emissivity of the atmosphere depending on precipitable water content (w) and performs well in the limit of a dry atmosphere:

$$L_{in} = \{1-(1+w)\exp(-(1.2 + 3.0\, w)^{1/2})\}\sigma T^4_a$$
$$w = 46.5\,(e_2/T_2$$

Clouds have a strong influence on long-wave radiation exchange because they are almost perfect radiators. The most common approach to estimate the effect of clouds upon the net long-wave radiation is to modify the cloudless sky value by a non-linear cloud term (Oke, 1987). If c is the fractional cloud cover, then net long-wave radiation flux is modified as:

$$L = \sigma \{1-(1+w)\exp(-(1.2+3.0\,w)^{1/2})\}T^4_a - \varepsilon_s T^4_a l.][1-c^2$$

Turbulent energy exchanges

Transportation of heat and moisture in the atmospheric surface sub-layer are governed primarily through turbulent motion. This transport gives rise to two forms of energy flux between the air and the snow/ice surface: Sensible heat flux (H) which is the direct transport of heat energy and Latent heat flux (LE) which is the transport of heat through the phase change of water. These fluxes play an important role in determining the rate of sublimation / melt form the surface.

(a) Sensible heat flux

The vertical turbulent sensible heat flux is expressed in flux gradient form as:

$$H = pC_p K_H (dT/dz - \Gamma) \quad (5)$$

Where p is the density of air, C is specific heat of the air (1005 J Kg^{-1} K^{-1}), K_H is the coefficient of turbulent diffusivity, dT/dz is the vertical temperature gradient and is the adiabatic lapse rate. As the present paper only deals with the air layer close to the glacier surface with large temperature gradients, Γ is neglected compared with dT/dz. Equation (5) can be reformulated in terms of simple data for wind speed and temperature following Ambach and Kirchlechner (1986) and Paterson (1994, p. 60-66):

$$H = (C_p P_0 / P_0) A Pu (T_a - T_s) \quad (6)$$

$$A = k^2 / [In (z_a / z_0)]^2 \quad (7)$$

Where p_0 is the density of air (1.29 Kg m^{-3}) at the standard atmospheric pressure P (101300 Pa), A is the dimensionless turbulent transfer coefficient (assumed here to be the same for transfer of either heat or water vapour) under neutral conditions (in which buoyancy effects are absent), P is the mean atmospheric pressure at the measuring site, u and T are measured wind speed and air temperature at measurement level z_3= 2 meter above the glacier surface, k is the von Karman constant (0.4) and z_0 is the aerodynamic roughness length.

(b) Latent heat flux

By analogy with the sensible heat flux, the latent heat flux is given by:

$$LE = Lv\,(0.623\,\rho_0 / P_0)\; A\,u\,(e_a - e_s) \qquad (8)$$

Where L is the latent heat of vaporization, e is the vapour pressure at height z above the glacier surface and e is the saturation vapour pressure at the glacier surface. The latter is a function of the surface temperature and is 611 Pa for a melting surface (Paterson, 1994, p. 65). e is calculated from the saturation vapour pressure over a plane surface of pure water using the Goff-Gratch formulation (List, 1971) and the prevailing relative humidity, e_s is assumed to be the same as the saturation vapour pressure over a plane surface of pure water at surface temperature T. We follow Ambach and Kirchlecchner (1986) in distinguishing between condensation and sublimation, i.e. with latent heat L = 2.514 and 2.849 MJ Kg^{-1}, respectively. When $(e_a - e_s)$ is positive and T = 0°C, water vapour condenses as liquid water on the melting glacier surface with Lv = 2.514 MJ Kg-1. When (ea -es) is negative, there is sublimation with L_v = 2.849 MJ Kg^{-1}. Also when $(e_a - e_s)$ is positive and $T_s < 0°C$, there is condensation from vapour to solid ice with L_v=2.849MJ Kg^{-3}.

The bulk transfer equations (6), (7) and (8) are valid only for neutral atmospheric conditions. However, in actual case the atmosphere above the snow or ice surface is seldom neutral. In that case appropriate stability corrections are applied for the transfer coefficient A in terms of Richardson number (R_i). Price and Dunne, 1976, showed that for stable conditions ($R_i > 0$), transfer coefficient is given by:

$$A_s = A/(1+10\,R_i.) \qquad (9)$$

Under unstable conditions ($R_i < 0$), the transfer coefficient can be modified by:

$$A_u = A(]-10\,R_i) \qquad (10)$$

Other workers (Hong, 1992; Rijan Bhakta and others, 1999) have used these correction factors with reasonable accuracy.

RESULTS AND DISCUSSION

Meteorological Conditions

Figure la shows the daily variation of ambient temperature over the two surfaces for Jan and Feb 1999. Over blue ice, measured average ambient temperature was -5. 6°C, while over shelf ice average T_a was -8[d].26 C. Thus average Ta over shelf was 2.66°C lower than over the blue ice which indicates the relatively large radiative heating of the blue ice surface. The variation pattern shows that a sharp rise in average air temperature corresponds to fair weather, followed by a drop in air temperature corresponding to bad weather days. One interesting feature to be noted is that variation in air temperature over both the surfaces followed each other although there seems to be time delay in the appearance of short-term temperature maxima at the two locations. The time delay patterns are classified into two groups. In one. the temperature maximum appeared earlier at blue-ice locationthan at she If (figure lb, events P1, P2 and P3). In the other, the temperature maximum at shelf location preceded that at blue-ice site (figure 1 c, events P4 and P5). In both cases the maximum propagated within one or two days. The nature of the delay pattern depends whether the centre of the low-pressure disturbance is closest to the shelf or blue-ice site.

Figure 1 d shows the daily variation of average relative humidity over the two surfaces for Jan and Feb 99. The average relative humidity was much higher over the shelf ice surface (average=69.8%, maximum=90.1%, minimum=52.4%) than that over the blue-ice surface (average=56.3%, maximum=81.6%, minimum=44.2%). This is quite expected because the shelf ice location represents typical coastal environment.

Figure 1 e shows the variation of monthly mean ambient temperature, surface temperature, relative humidity and wind speed from Feb 99 to July 99 over blue-ice. A remarkable feature was the temperature rise in June, otherwise the air temperature continued to drop with the onset of austral winter. The phenomenon of the winter temperature having no distinct minimum is known as a "coreless" winter for the Antarctic (Meinardus, 1938). Average surface temperature was lower than average air temperature for all months except Feb 99. This is because of longer period of unstable stratification caused by strong radiative heating of the ice surface during month of Feb. Wind speed was highest in June with an average value of 9.24 m/sec.

Radiation Characteristics

Short-wave radiant flux (insolation), transmissivity and cloudiness

We define an effective transmissivity of the atmosphere ($_{eff}$) as the ratio of daily totals of incoming short wave radiation and extraterrestrial radiation 1 on a horizontal surface:

$$\tau_{eff} = S_{in}(\downarrow) / I \qquad (11)$$

The result of a number of atmospheric processes, that is, scattering and absorption of solar radiation by air, aerosol and clouds is included in $_{eff}$ Daily mean values of S_{in} (↓) from Feb to April 99 over blue-ice are plotted in figure 2a, together with extraterrestrial irradiance, I. $_{eff}$ varies between 0.21 to 0.89, having a mean value of 0.63 (figure 2b). These variations are mainly due to differences in cloudiness (figure 2c). Table 1 lists monthly mean values of S_{in}(↓), I and $_{eff}$ (the last three columns are explained later).

Albedo over continental shelf and blue ice

We define daily albedo as the ratio of daily amount of reflected solar radiation to the daily insolation. Note that this differs from the daily mean albedo, which is mean of all instantaneously determined albedo values during daylight. However, when the solar elevation angle is very low, this quantity may be influenced greatly by instrumental errors. In view of this we will concentrate on daily albedos for analysing measurements.

Figure 3a shows the daily variation of albedo over both the surfaces during Jan and Feb 99. The plot shows that albedo over shelf is much higher than over blue ice as the albedo over shelf is due to snow while over blue ice it is due to ice only. The average albedo over continental shelf is 82.4 % while that over blue ice is 60.9 % for the corresponding period. These values are in general agreement with those reported by various investigators. Figure 3b shows daily albedos from Feb to April 99 over blue-ice. Also shown in the figure 3b are the days with snowfall events. As expected, there is a clear relation between albedo and snowfall events. The monthly mean albedos are given in Table 1. The last two columns in Table 1 shows the absorbed solar radiation A and efficiency of absorbing solar radiation (f) defined as

$$f = A / I \qquad (12)$$

So, f indicates how much of the insolation at the top of the atmosphere is actually being absorbed at the blue-ice surface. In the 6 monthly mean. only 23 % of the extra-terrestrial irradiance would be absorbed by a horizontal surface over blue-ice at the AWS site.

Albedo variation with solar elevation angle and cloud amount

Decrease in albedo values has been observed on clear sky days with increase in solar elevation angle. Figure 4a shows the diurnal variation of albedo over the continental shelf. At low elevation angle photons strikes the surface at grazing incidence resulting in high albedo. The albedo values have been observed to follow diurnal hysteresis pattern i.e. higher values in morning hours than in afternoon hours for the same elevation angle. This may be attributed to the formation of thin, weak coating of hoar-frost layer in the morning and evening hours and changes in surface morphology and wetness during day time, Figure 4b shows the diurnal pattern observed over the blue-ice in the month of April 1999.

The albedo values are found to increase with increase in the cloud amount, as shown in figure 4c. The increase in albedo can be attributed to the fact that cloud absorbs a larger part of infrared than visible radiation. Thus, a relatively larger portion of visible radiation reaches the surface under cloudy condition. Since, the albedo in the visible range is very high compared to near IR albedo, an increase in surface albedo is to be expected during overcast conditions. Figure 4d shows the variation of daily albedos with mean daily cloud amount (values are averaged as a function of cloud amount). We hesitate to give a full analysis, as we have not considered the type of clouds.

Albedo measurements over Sea-Ice

The albedo of sea ice was investigated during the sea voyage to Antarctica, through pack ice in the southern ocean. The time of observation was close to mid-summer. For the period of 8th Jan 1999 to 13th Jan 1999, continuous radiation and meteorological measurements were carried out from the ship. On 9th Jan 1999, the first sea ice was seen. All solar radiation data were measured with Kipp & Zonen pyranometer and recorded on a SUTRON 8210 scientific data logger.

The mean diurnal variation of the global and reflected radiation for the mean of observation period is presented in Figure 5a. Daily courses for individual days varied widely, depending mostly on the amount and type of cloud and to a lesser extent on the atmospheric turbidity. A maximum mean daily value of 225 W/m- was observed on 12th Jan 1999, a partly cloudy day, the minimum (140 W/m-) was observed on 11th Jan 1999.

with complete overcast. The mean daily radiation was measured as 201 W/m2 and was strongly dependent on the amount of cloudiness.

For open water. albedo values varied between 7% and 16%. The exact value depended on the solar elevation, the absence or presence of clouds and the sea-state. The sea ice we encountered was normally covered with snow. Values of up to 80% were recorded as mean hourly values for 10/10 snow covered sea ice. In Figure 5b the ice concentration which has been observed hourly is plotted against the reflectivity. It can be seen that the albedo increases with increasing ice concentration. Ice concentration and albedo were averaged for 2-10 ice concentration classes. For open water, a mean value of about 12% was observed. This relatively high value is may be because of long time periods with low solar elevation during which the surface reflectivity is increased. For 10/10 sea-ice concentration, the mean albedo value was 61%. The mean value for the albedo for the whole observational period was 43%. The observed values are in agreement with those reported previously.

Surface Energy Balance

The surface energy balance over Antarctic snow surfaces has been extensively studied, e.g. Wellor (1980) and Wendler and others (1988). However, the energy balance of blue-ice areas is relatively unknown. Fujii and Kusunoki (1982) attempted to relate calculated blue-ice sublimation rates to measured values but treated only the latent heat flux. Bintanja and van den Broeke (1994) considered all the energy fluxes but analysis period was restricted to austral summer. In this paper we will evaluate the surface energy budget components both on blue-ice and snow (continental shelf) for the late summer period. We will also compare the summer and winter energy balance over blue-ice surface.

The full energy balance was calculated on an hourly basis. Aside from being physically more correct than a daily calculation, the hourly calculation of the turbulent fluxes has a hidden bonus. This is because the temperature sensors show a clear sign of radiation heating; temperatures rise quickly if wind speeds drop below about 1.5 m/sec. This caused some concern until it was realised that, even if the temperature is erroneously high for a particular hour, it is multiplied by a correspondingly low wind speed for the same hour so that the resulting error in sensible heat, averaged over the day will be small because the largest contributions come from hours with relatively high wind speeds. The hourly values of computed energy balance are summed into daily totals and averaged over the late summer and winter period.

Mean surface energy fluxes and mean albedo for the period 19 January-28 February 1999 over snow and blue-ice are given in Table 2. Due to the differences in

albedo, the blue ice surface has greater net short wave radiation at the surface. Averaged over the analysis period, surface temperature is slightly higher over blue ice than snow. leading to slightly greater long wave loses over blue ice surface. For snow surface, net long-wave radiation (L) emitted is comparable with net short-wave radiation thereby making the net radiation (R_{net} very small. However, R_{net} over blue-ice is quite high and positive, making it a significant heat source term. Sensible heat flux over snow is on an average positive (the air warms the surface) in contrast to that over the blue-ice surface. The latent heat flux is on an average negative over both the surfaces, indicating evaporation is more prevalent than condensation. The latent heat flux over snow is much less than that over blue-ice; which is quite expected. Overall energy budget is negative over both snow and blue-ice surfaces. One should note that we have not considered the energy exchange due to other agents e.g. precipitation or wind drift activity.

We will now present the heat budget analysis over blue ice for the late summer and winter periods. Late summer values are mean for Feb and March and winter values for June and July (Table 3).

The time series of net short wave and net long-wave fluxes for late summer period are shown in figures 6a and 6b respectively. It can be seen that net short-wave budget steadily decreased from 85.68 Wm^{-2} in Feb to 35.2 Wn^{-2} in March with average value of 60.4 $W m^{-2}$ for the summer period. In contrast to the summer period, the short wave balance during June and July is almost zero as the solar disc is always below the horizon. There is a decreasing trend in long wave loses from Feb to March with average value of-43.9 Wnr- for the summer period, which is strongly affected by the presence of fractional cloud cover. In figure 7, the net long wave radiation is plotted against fractional cloud cover. While the mean value for 8/8 cloudiness was -26 Wm^{-2}; the losses more than doubled for clear sky conditions with average value of-60 Wm^{-2}. Values were averaged as a function of fractional cloud cover. Instead of a linear regression, a polynomial function of order four was found more suitable to fit the variation in the calculated values. The time series of net long wave radiation during winter period is shown in figure 8a and the average value was found to be -26.8Wm^{-2}.

The average net radiation was positive (flux towards the surface) during the late summer period and changes sign between seasons. The time series of net radiation for late summer period is shown in figure 6c. While the average value for Feb was 35.9 Wm^{-2} it was reduced to -2.9 Wm^{-2} in March with average value of 16.5 $W m^{-2}$ for the summer period. During winter the net radiation balance consists of only long wave budget and is a strong sink term. The time series of net radiation during winter is shown in figure 8a. Compared to the average value of 16.5 $W m^{-2}$ in summer the average value in winter was -26.8 Wm^{-2} (strongly negative).

The sensible heat-flux also changes sign and shows an increasing trend between seasons. The time series of sensible heat flux for summer is shown in figures 6d, In Feb. average value was-13.4 Wm^{-2} (flux away from the surface) while in March it was slightly positive: 0.8 Wm^{-2} (flux towards the surface). The plots show a large positive as well as negative fluctuations, still the average values were small compared to these fluctuations. During Feb month, the chief turbulent production mechanism is buoyancy of the surface layer due to strong heating of the ice. Warming of ice is very effective through a large penetration depth for ice and low back scattering coefficient for the large grained blue ice surface. Larger surface heating causes a longer period of unstable stratification, which is indicated by a negative sensible heat flux in Feb. The time series for the winter period is shown in figure 8b. The average value in winter, 35.9 Wm^{-2}, was quite high compared to summer period. Thus during late summer period sensible heat flux acts as a weak sink term while in winter it is strongly positive and acts as a source term.

The surface gains latent heat when atmospheric water vapour condenses on it and loses heat when moisture evaporates from it. Process of sublimation/evaporation was found to play an important role over blue ice in suppressing summer ablation/melting, since required heat by sublimation of ice is about 8 times as large as that by fusion. Present analysis shows that latent heat flux is one of the dominant components of the energy balance. The time series of latent heat flux for late summer and winter periods are shown in figures 6e and 8c respectively. Latent heat flux was found to be negative in both summer and winter period (i.e. fluxes are away from the surface) though the winter loses (average value - -40.1 Wm^{-2}) are less than that in summer (average value - -59.3 Wm^{-2}). Although latent heat flux is a function not only ofnet radiation but also of met parameters, it is most strongly influenced by the net radiation. Figure 9 shows their relationship over blue ice. It can be seen that latent heat loses from the surface increases with increasing net radiation.

The surface energy budget is the net flux into or out of the snow/ice surface. It might be used for phase change (melting or sublimation) or storage change (change of temperature of ice sheet or snow layer). The time series variation of surface energy budget for summer and winter are depicted in figures 6f and 8d respectively. The values are positive as well as negative with average value of 49.2 Wm^{-2} for summer and -30.9 Wm^{-2} for winter period.

The mean daily variation in each of the energy balance components is large and can vary considerably. The average diurnal cycle of short wave and long wave radiation, sensible heat flux, latent heat flux and surface energy budget for the month of Feb at blue ice site is depicted in figure 10. Short wave radiation peaks at near 230 Wm^{-2} at 1100h (approximate local solar noon) and then drops to a minimum at about 2000h. This is the driving force for the latent and sensible heat fluxes, which show similar

diurnal cycles. Latent heat varies from -55 to -90 Wm^{-2} with the greatest flux at solar noon when air temperature is greatest and therefore can drive the greatest vapour exchange. The large surface heating causes a longer period of unstable stratification indicated by negative sensible heat flux during daytime. Since the radiation fluxes are higher than the turbulent heat fluxes in Feb, it is obvious that the overall surface energy budget will also follow the diurnal pattern of net radiation. The surface energy budget was positive between 0900 hrs and 1500 hrs UTC i.e. surface was gaining energy between this period. For the remaining part of the day surface was continuously losing energy. The surface energy budget was found to fluctuates between 40 to-100 $W m^{-2}$.

CONCLUSIONS

Results are presented from measurements carried out in the general area of Dronning Maud Land in East Antarctica during XVIIIth Indian Scientific Expedition to Antarctica. Two AWS were installed over continental shelf and continental ice (blue-ice) surfaces and detailed meteorological measurements were carried out on blue-ice as well as on snow. The albedo of sea-ice in the southern ocean was also investigated. The mean albedo varied from 12 % for open water to 61 % for 10/10 sea-ice concentration.

The surface energy balance is evaluated using a simple model and measured meteorological parameters. The differences in the surface energy balance between snow and blue-ice (larger net short-wave radiation accompanied by larger negative contribution of net long-wave radiation, and turbulent fluxes) can be attributed mainly to differences in albedo, surface roughness, thermal conductivity and short-wave extinction coefficient (Bintanja and others, 1994). It appears that the main difference in summer and winter budget is in the net radiation and sensible heat balance. While the net radiation balance decreases from 16.5 $W m^{-2}$ in summer to -26.8 $W m^{-2}$ in winter, the sensible heat budget increases from -6.3 Wm^{-2} to 35.9 $W m^{-2}$ in the corresponding period. It is apparent that net radiation is the dominant energy source and latent heat flux is the dominant energy sink in the late summer period. On the other hand it is the sensible heat flux, which is major energy source, and latent heat flux and net radiation are the major energy sink in the winter period. On average, sensible heat flux provides the net energy for the sublimation during the winter period. While in summer the excess energy from the net radiation is used primarily for sublimation.

Since stakes were not put up at the experimental sites, it was not possible to measure physically the ablation/accumulation over the two surfaces. Also lack of instruments to measure the turbulent fluxes made it impossible to measure the fluxes physically. Thus the results obtained regarding the turbulent fluxes are calculated values which were derived from data that was collected with reasonable accuracy and frequency. This paper highlights the fact that turbulent fluxes play a significant rote in

the overall surface energy budget of this icy continent and proper instrumentation to measure the turbulent fluxes as well as stake measurement are necessary to actually test the validity of the energy budget formulation used by us.

ACKNOWLEDGEMENTS

I would like to thank National Centre for Antarctic and Ocean Research (NCAOR) for providing the opportunity to participate in the expedition. I am grateful to expedition leader Sri Ajay Dhar and all members of XVIII SEA for providing the logistic support and co-operation during the expedition. I also express my sincere gratitude to Maj Gen SS Sharma, KC, VSM, Director SASE and Sri DN Sethi, Deputy Director, SASE, for their kind encouragement and constant guidance during the course of the project.

Table 1. Solar radiation characteristics in monthly mean values. $S_{in}(\downarrow)$ is insolation, I is extraterrestrial irradiance, $_{eff}$ is effective transmissivity, A is absorbed solar radiation radiation, f is absorbed solar radiation scaled by extraterrestrial irradiance. In this table, albedo is the ratio of monthly mean reflected to incoming radiation

Month	$S_{in}(\downarrow)$ W/m^2	I W/m^2	$_{eff}$	A W/m^2	Albedo	f
February 1999	208	317	0.66	85	0.59	0.27
March 1999	103	179	0.58	34	0.66	0.19
April 1999	40	58	0.67	13	067	0.23
May 1999	0	0	-	-	-	-
June 1999	0	0	- '	-	-	-
July 1999	0	0	-	-	-	-
6 Monthly	117	185	0.63	44	0.64	0.23

Table 2 - Energy balance results over continental shelf and blue ice

Analysis period - 1 9 Jan to 28 Feb 1999

Energy balance components	Continental Shelf	Continental ice
Q_{sw} (W/m^2)	43.2	85.7
$Q1_w$ (W/m^2)	-44.9	-49.8
R_{net} (W/m^2)	-1.7	35.8
H (W/m^2)	7.3	-13.4
LE (W/m^2)	-28.2	-67.2
B (W/m^2)	-22.6	-44.7

Table 3 - Energy balance results over continental ice

Analysis period - Late summer and winter period

Energy balance components	Late summer	Winter
Q_{sw} (W/m^2)	60.4	0
$Q1_w$ (W/m^2)	-43.9	-26.8
R_{net} (W/n^2)	16.5	-26.8
H (W/m^2)	-6.3	35.9
LE (W/m^2)	-59.3	-40.1
B (W/m^2)	-49.2	-30.9

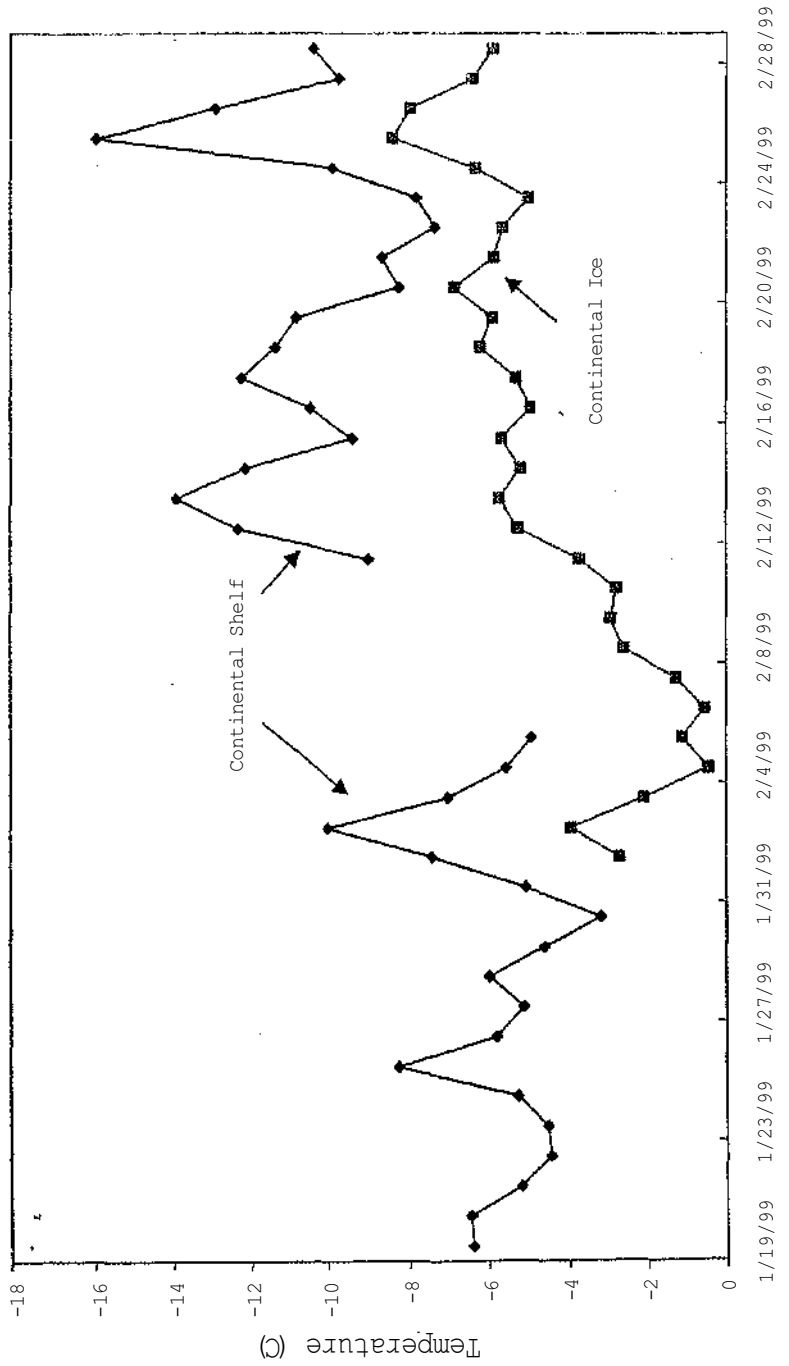

Figure 1a: Comparison of ambient temperature over continental shelf and continental ice

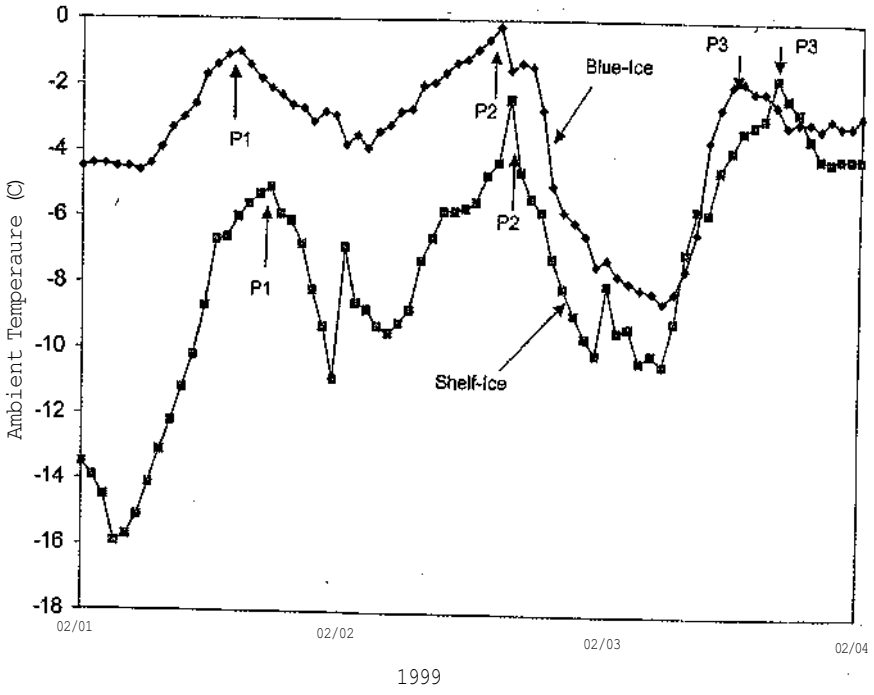

Figure 1b: Time delay pattern in short-term temperature maximum (P1, P2 and P3)

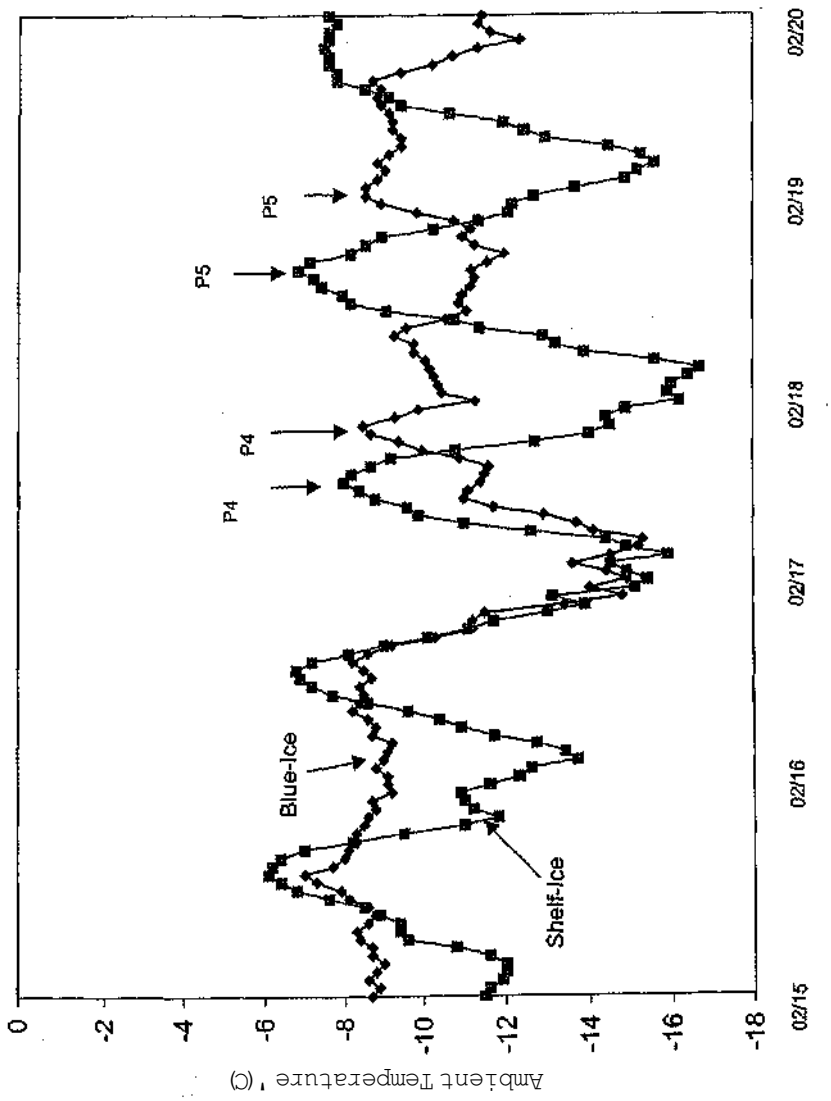

Figure 1c: Time delay pattern in short-term temperature maximum (P4 and P5)

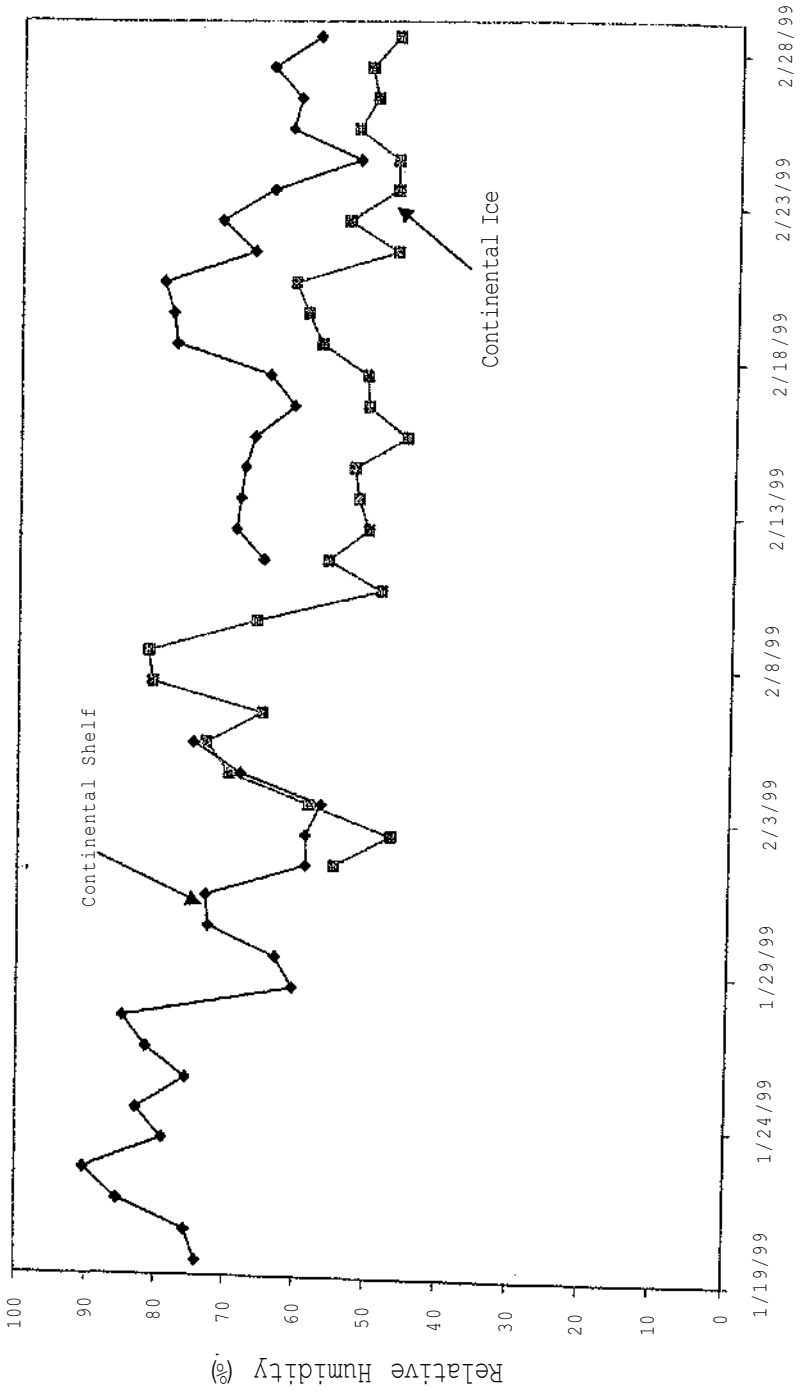

Figure 1d: Comparison of relative humidity over continental shelf and continental ice

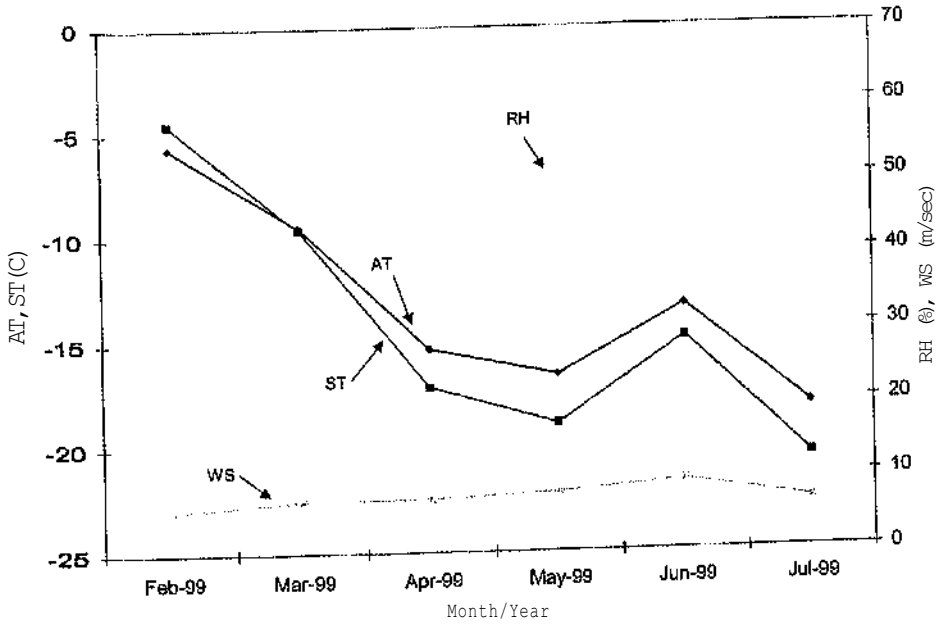

Figure 1e: Monthly variation of ambient temperature, surface temperature, relative humidity and wind speed

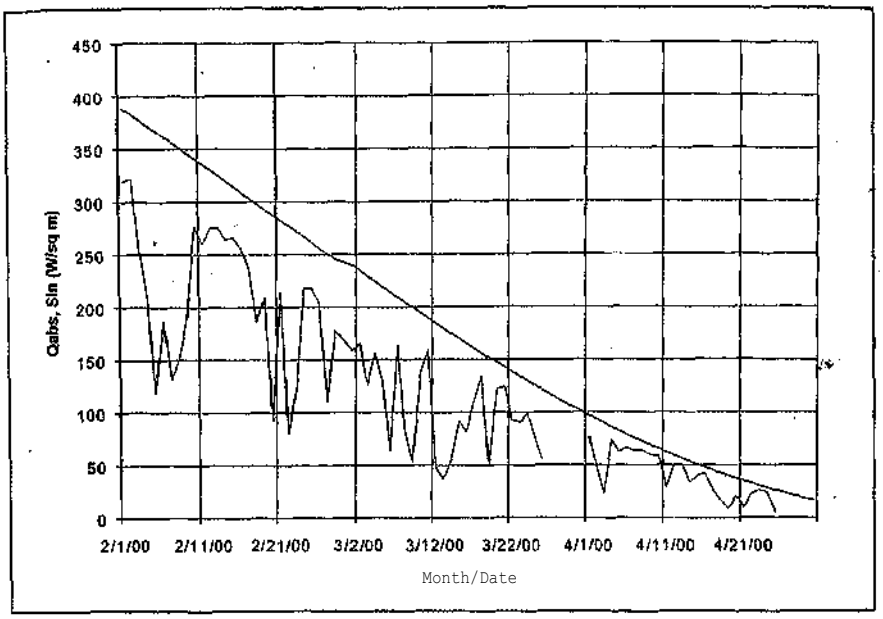

Figure 2a: Daily mean value of insolation and extraterrestrial radiation over blue ice

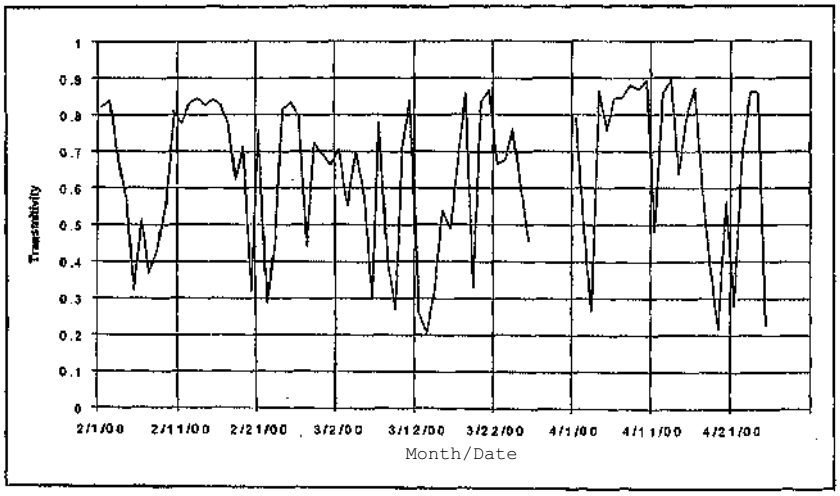

Figure 2b: Daily variation of effective transmissiivity over blue ice

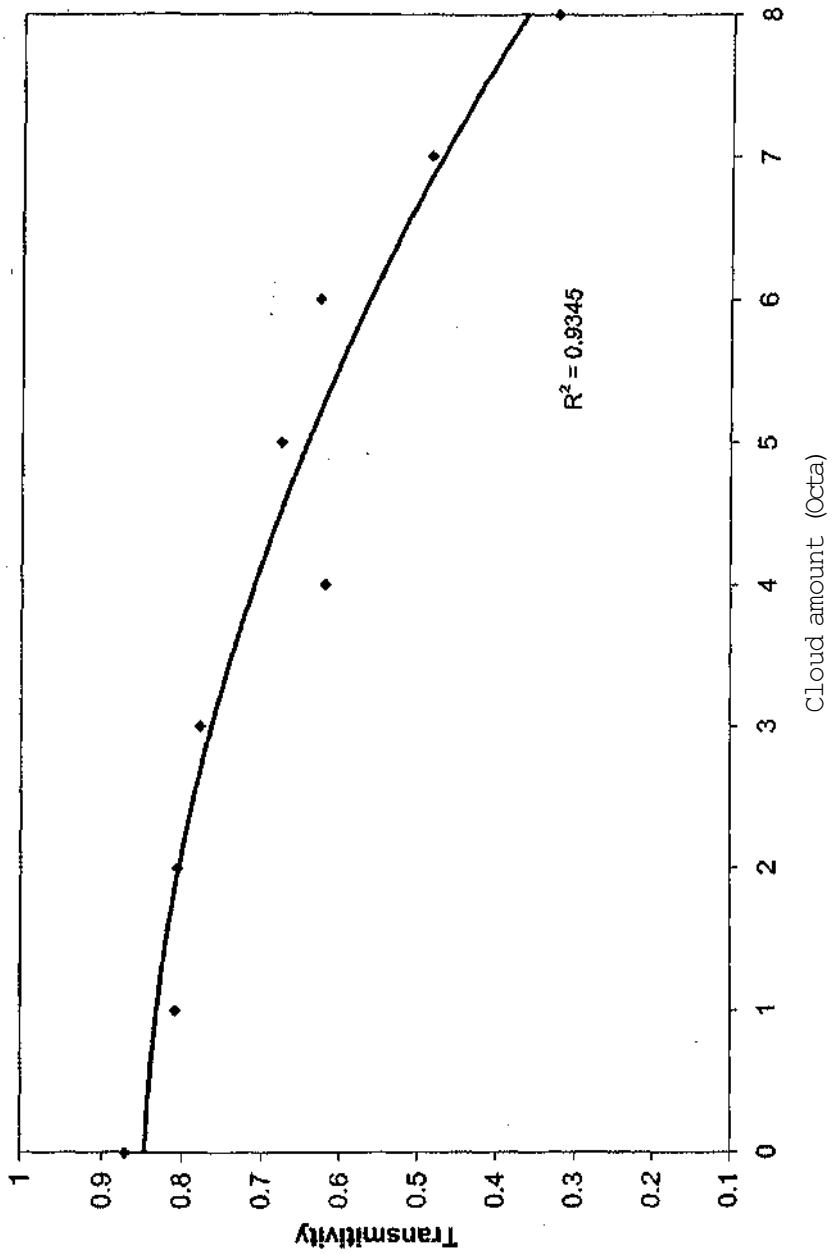

Figure 2c: Variation between effective transmissivity and cloud amount

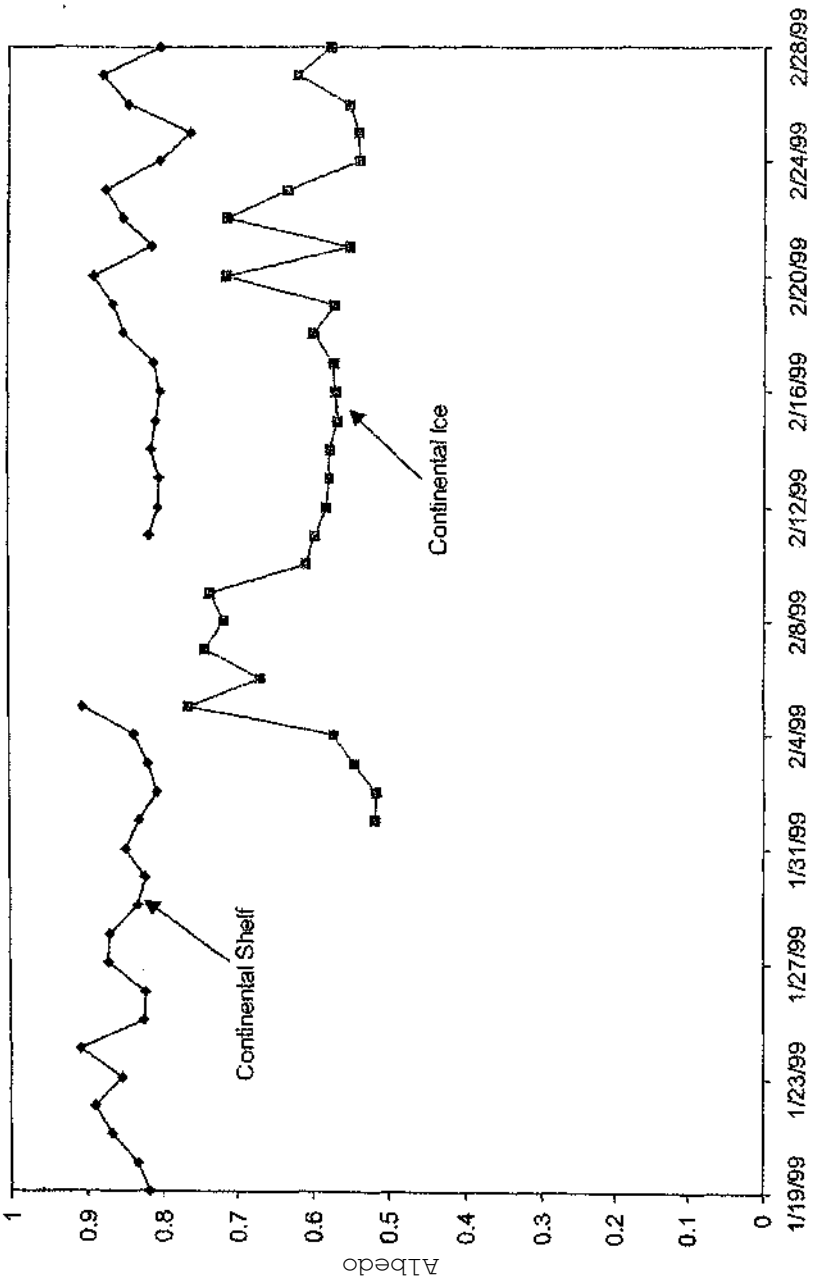

Figure 3a: Comparison of albedo over continental shelf and continental ice

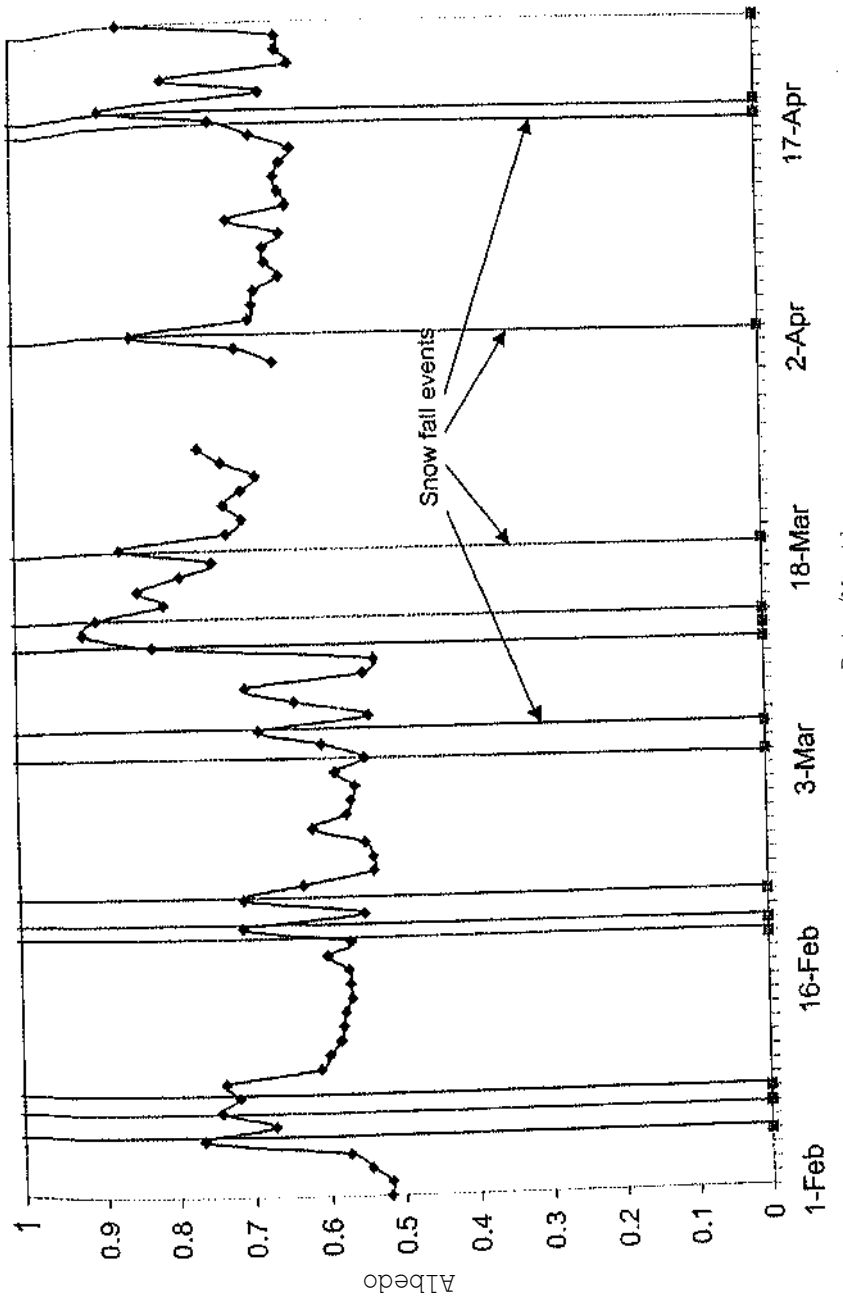

Figure 3b: Daily albedo over blue ice from Feb April 1999

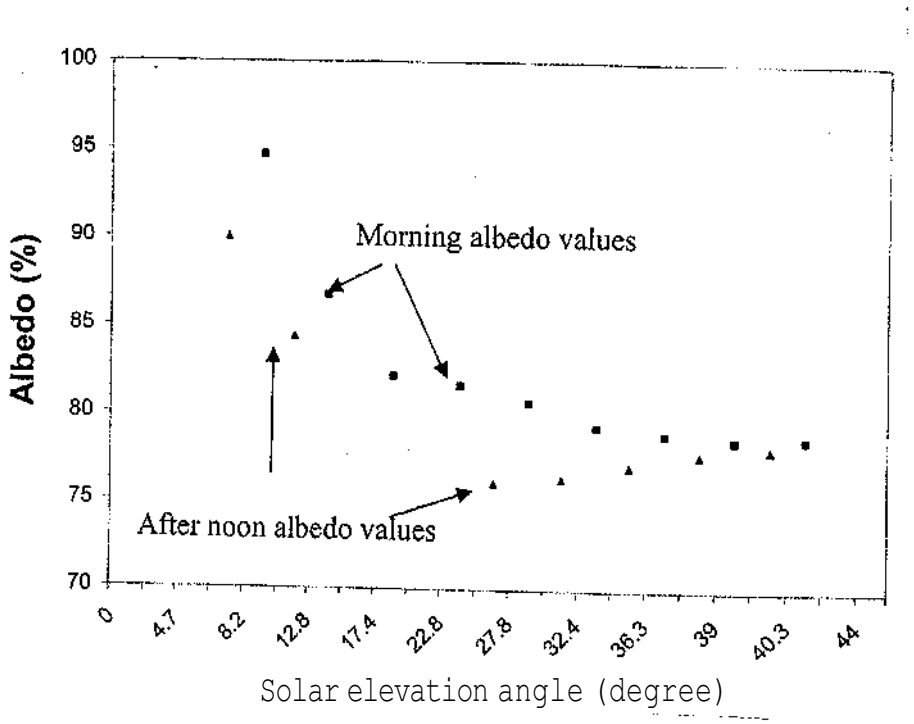

Table 4a - Diurnal loops observed in snow under clear sky conditions plotted as a function of solar elevation angle

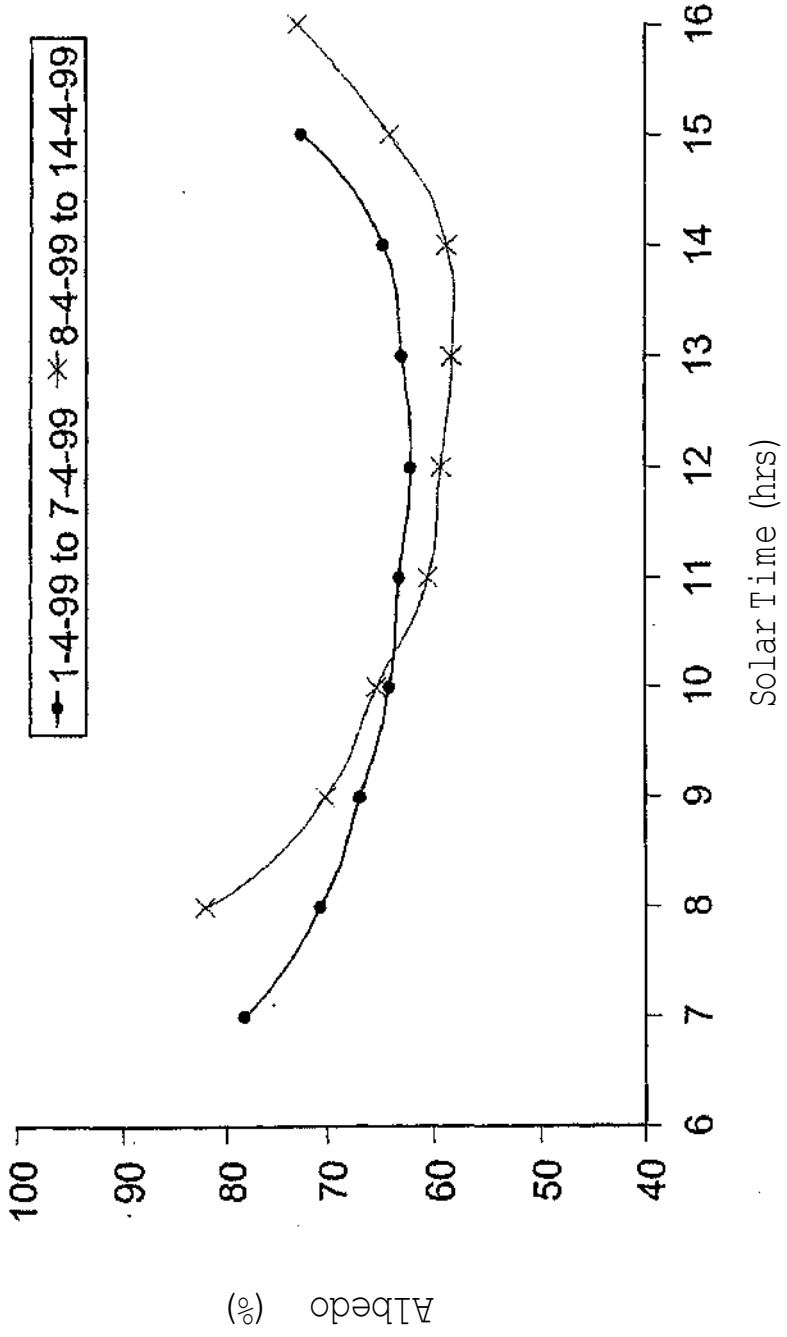

Figure 4b: Diurnal variation of albedo over blue-ice surface (Avg. Values)

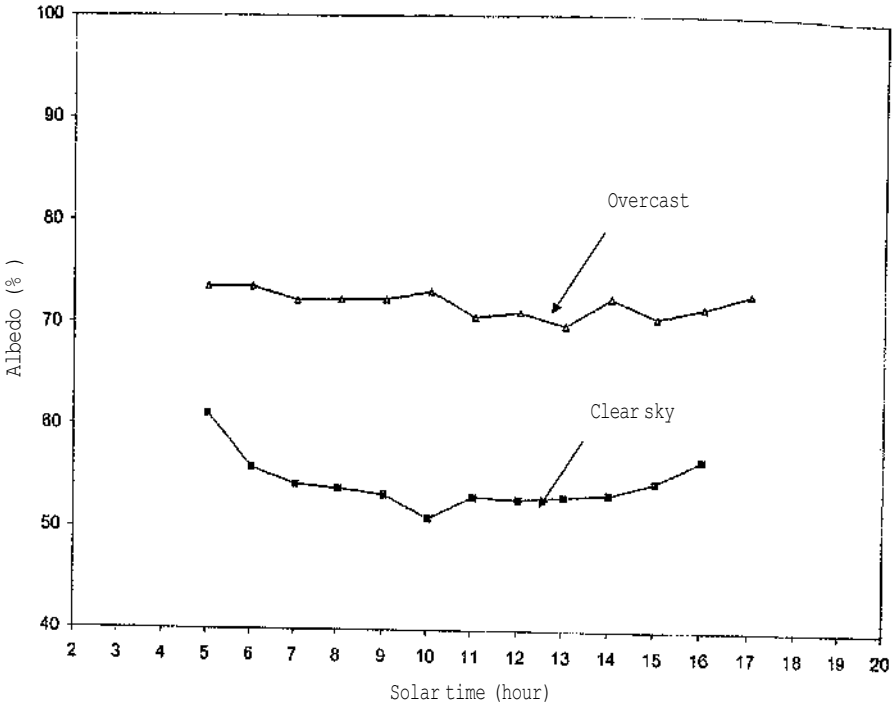

Figure 4c: Mean hourly variations of albedo values over continental ice for clear sky (0 to 1 octa) conditions and complete overcast conditions (7 to 8 octas)

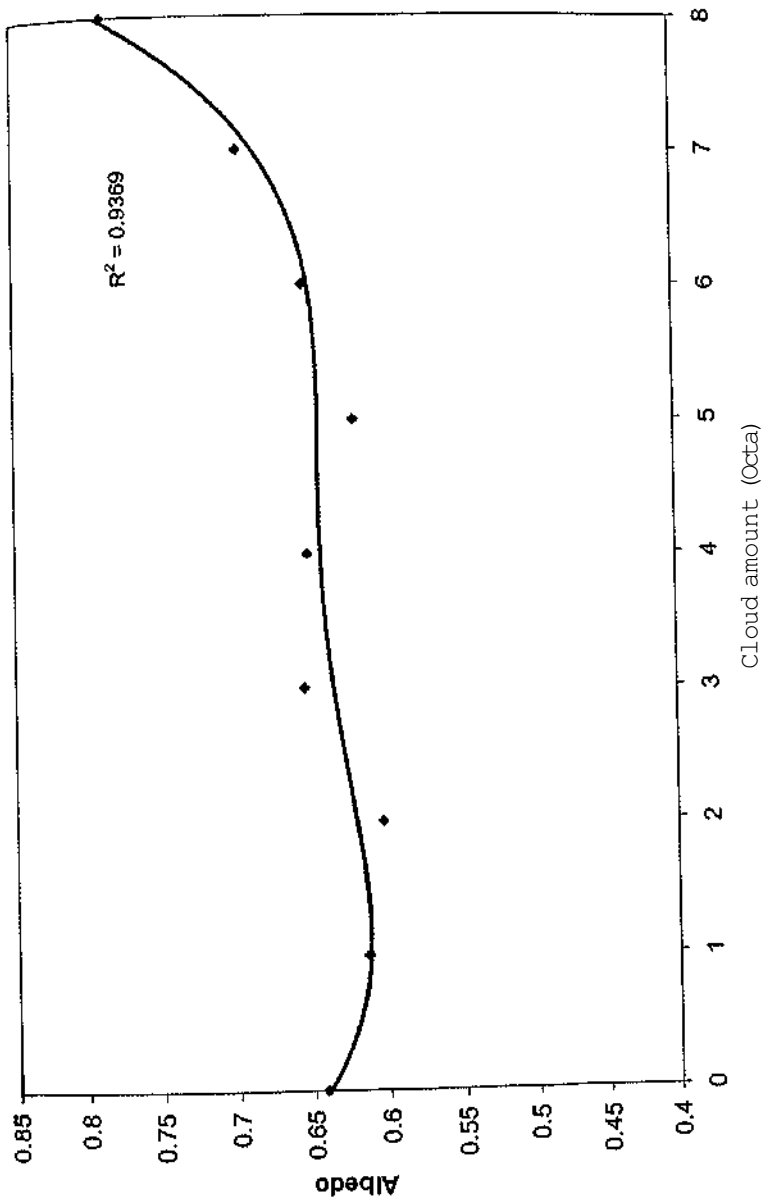

Figure 4d: Variation of daily albedo with mean daily cloud amount (values are averaged as a function of cloud amount)

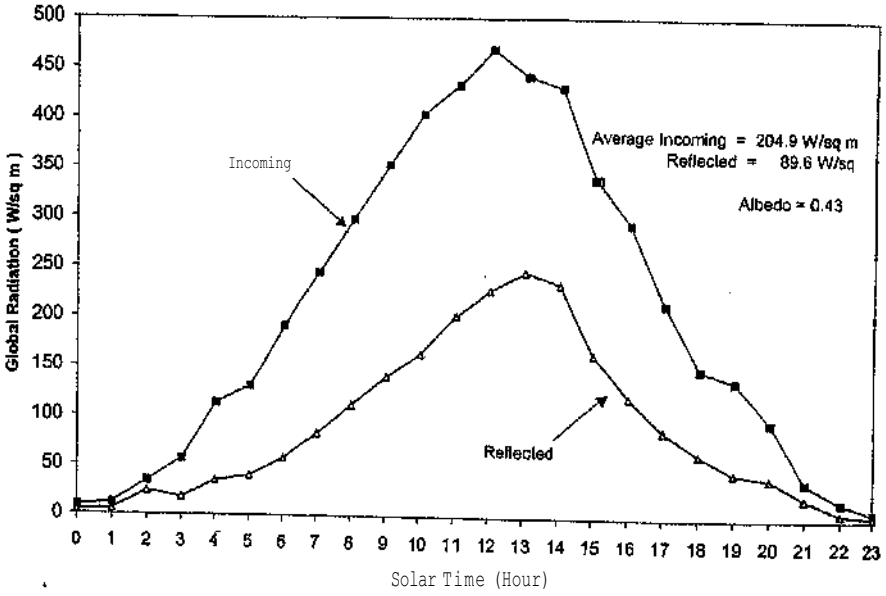

Figure Sa: M e m diurnal variation of global and reflected radiation over Sea Ice for the observation period

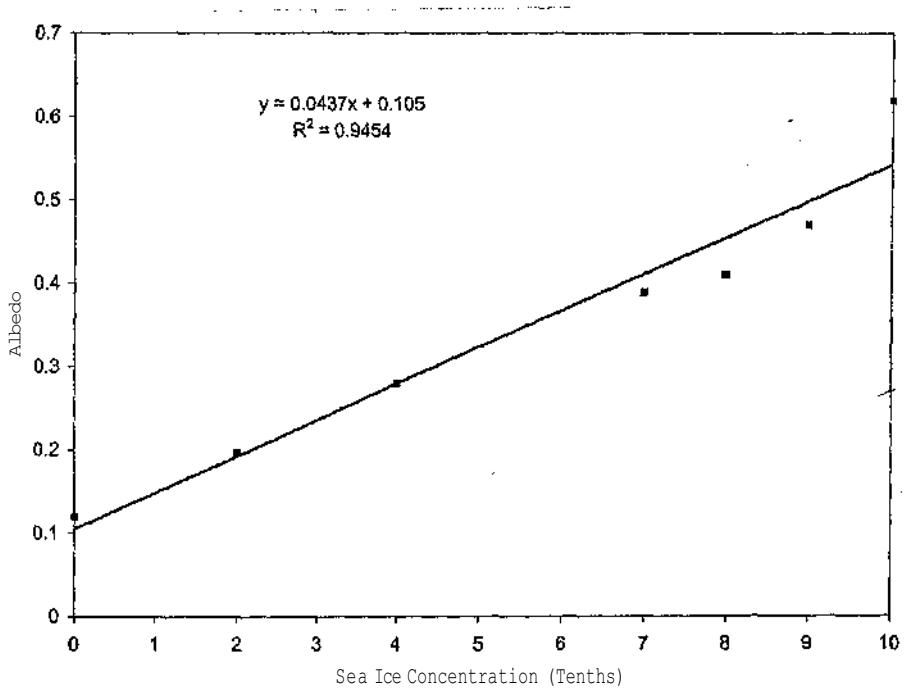

Figure 5b: The surface albedo as a function of sea ice concentration. Values are averaged as a function of ice concentration.

(a)

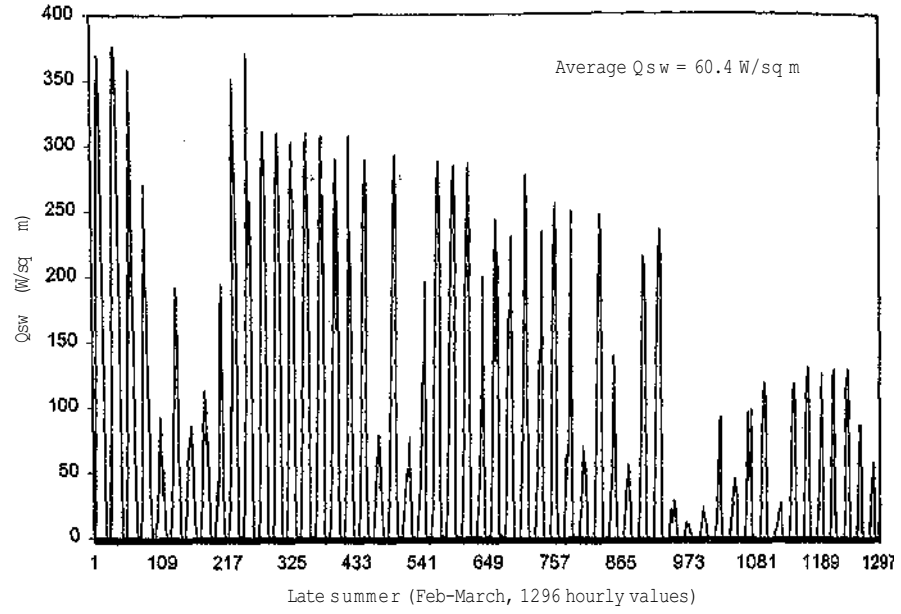

(b)

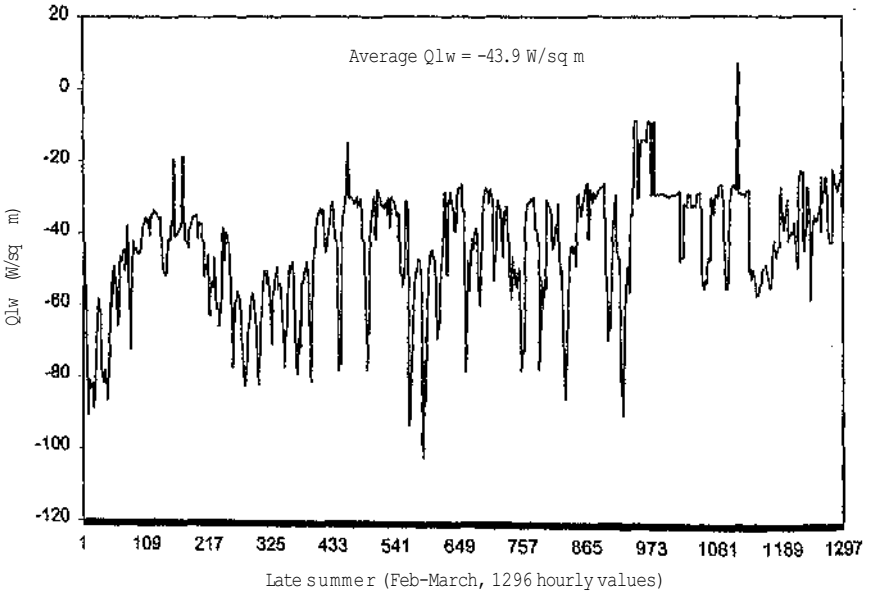

Figure 6 - Time series of surface energy budget components (a) Net short wave radiation, (b) Net long wave radiation for the late summer period

(c)

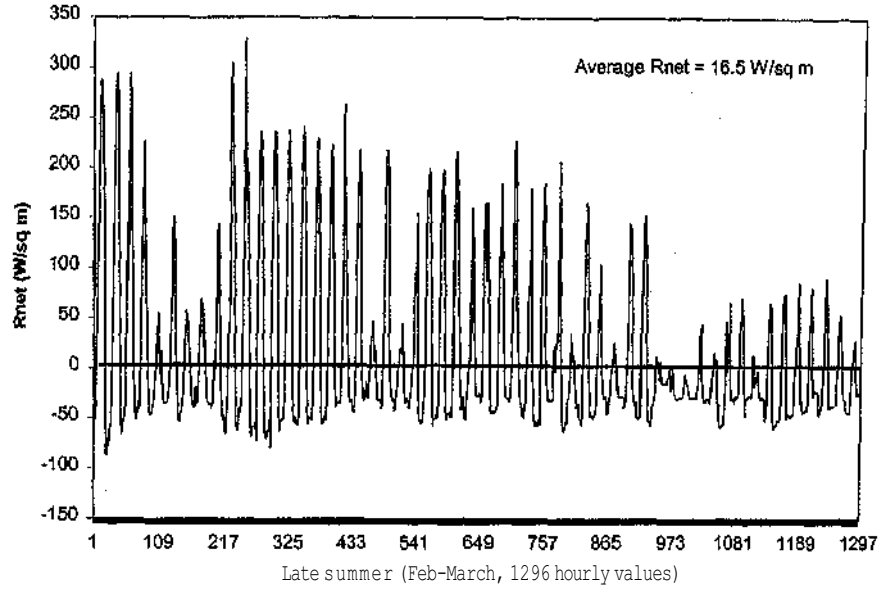

(d)

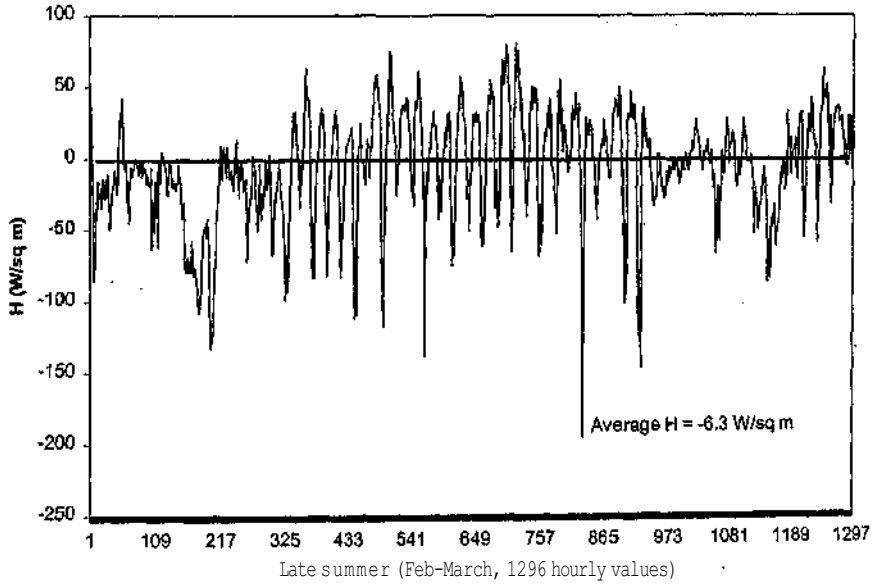

Figure 6 - Time series of surface energy budget components (c) Net radiation, (d) Sensible heat flux for the late summer period

(e)

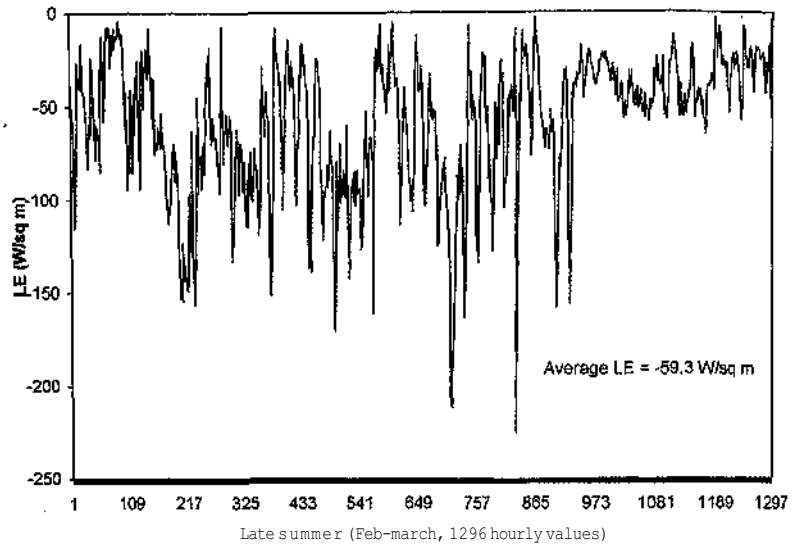

(f)

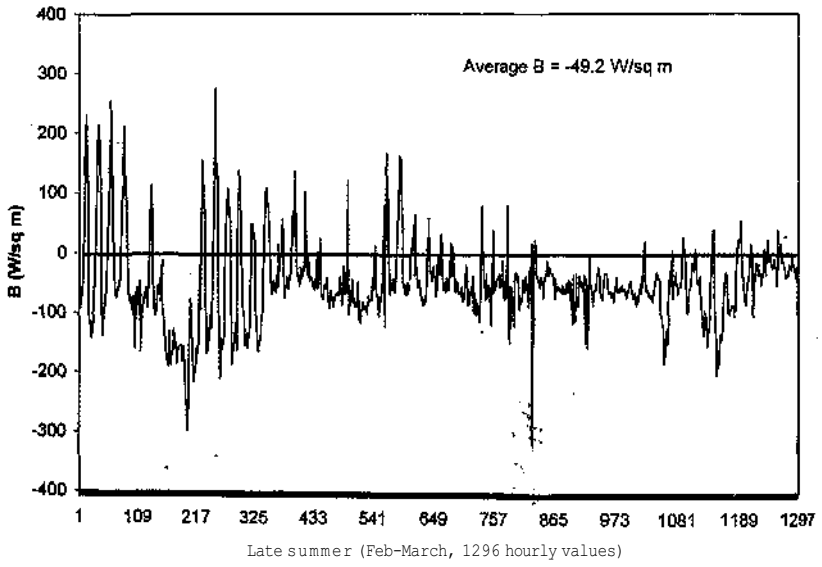

Figure 6 - Time series of surface energy budget components (e) Latent heat flux, (b) Net surface energy budget for the late summer period

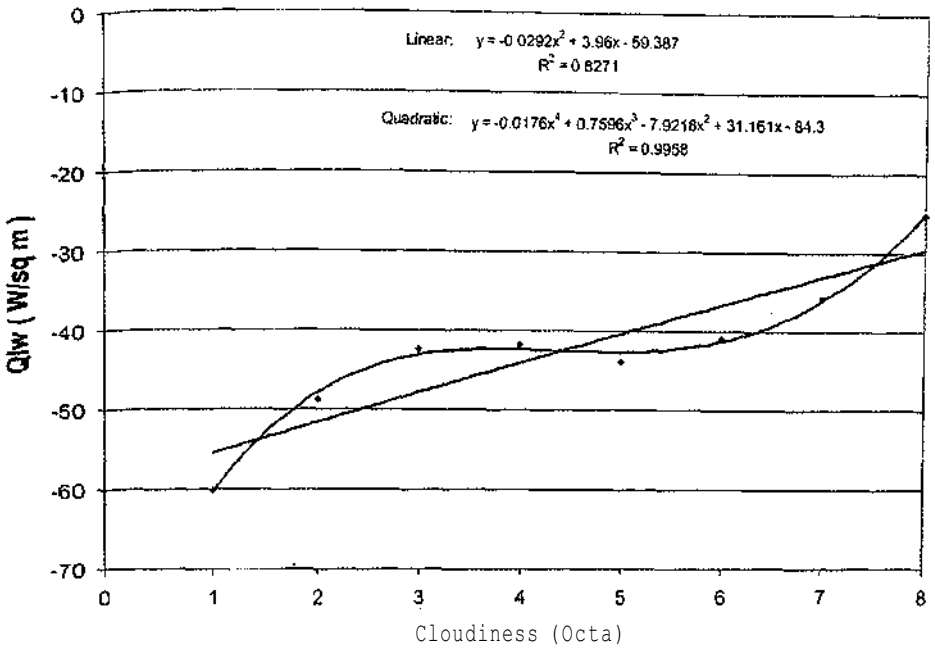

Figure 7: The long-wave radiation budget as a function of cloud amount, (values are averaged as a function of fractional cloud cover)

(a)

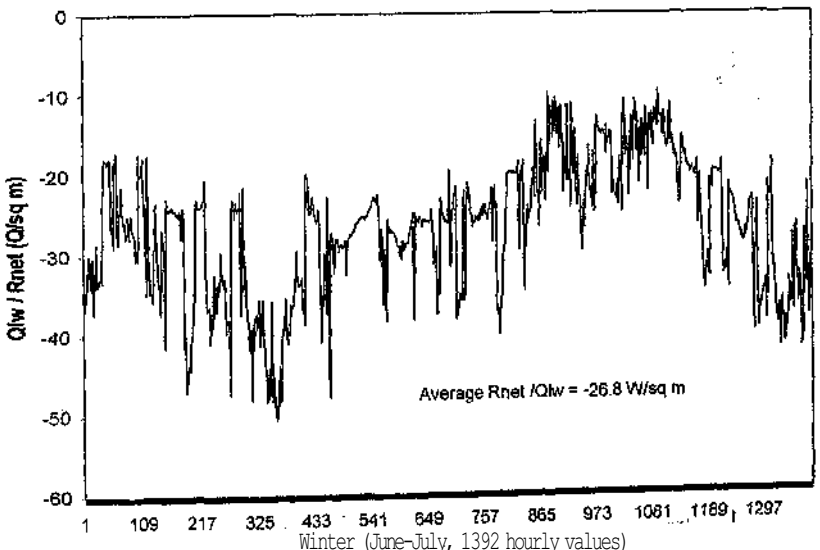

Winter (June-July, 1392 hourly values)

Figure 8 -Time series of surface energy budget components (a) Netlong wave radiation/Net radiation, (b) Sensible heat flux for the winter period

(b)

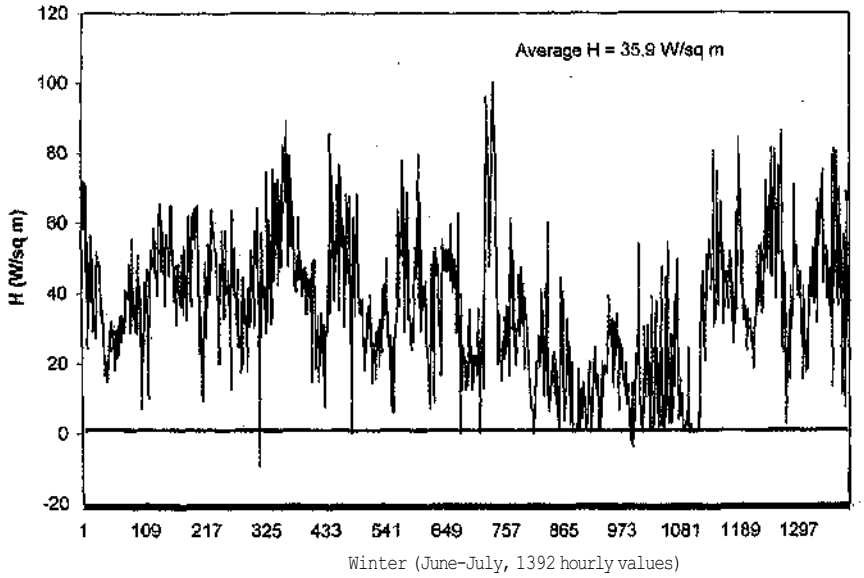

Figure 8 - Time series of surface energy budget components (a) Net long wave radiation / Net radiation, (b) Sensible heat flux for the winter period

(c)

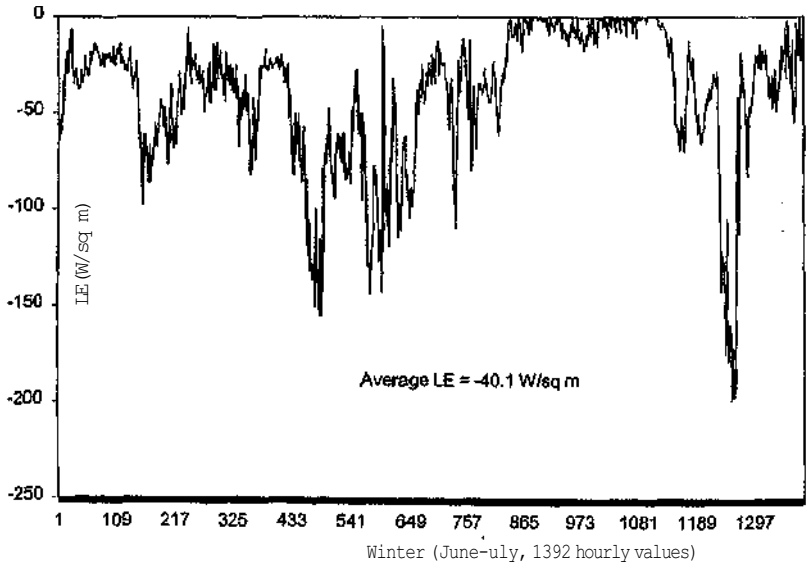

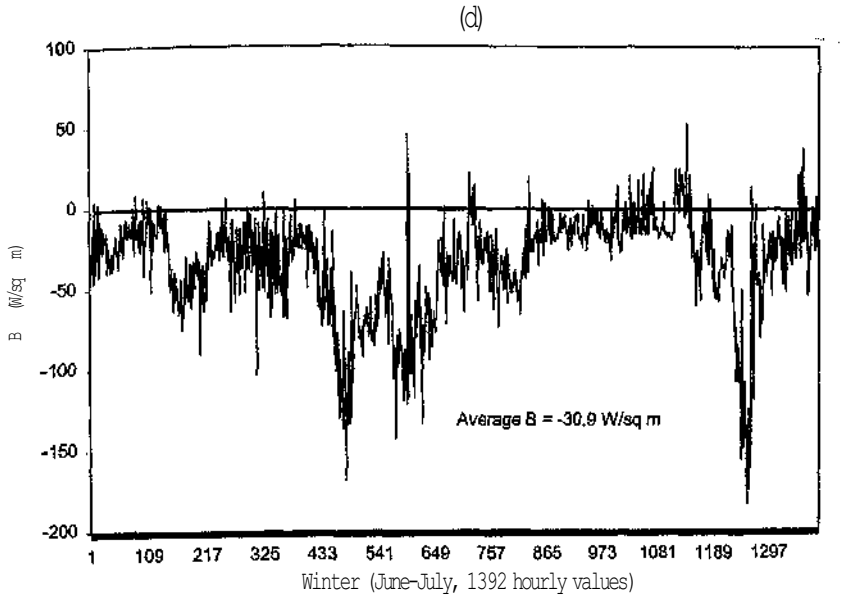

Figure 8 - Time series of surface energy budget components (c) Latent heat Flux, (d) Net surface energy budget for the winter period

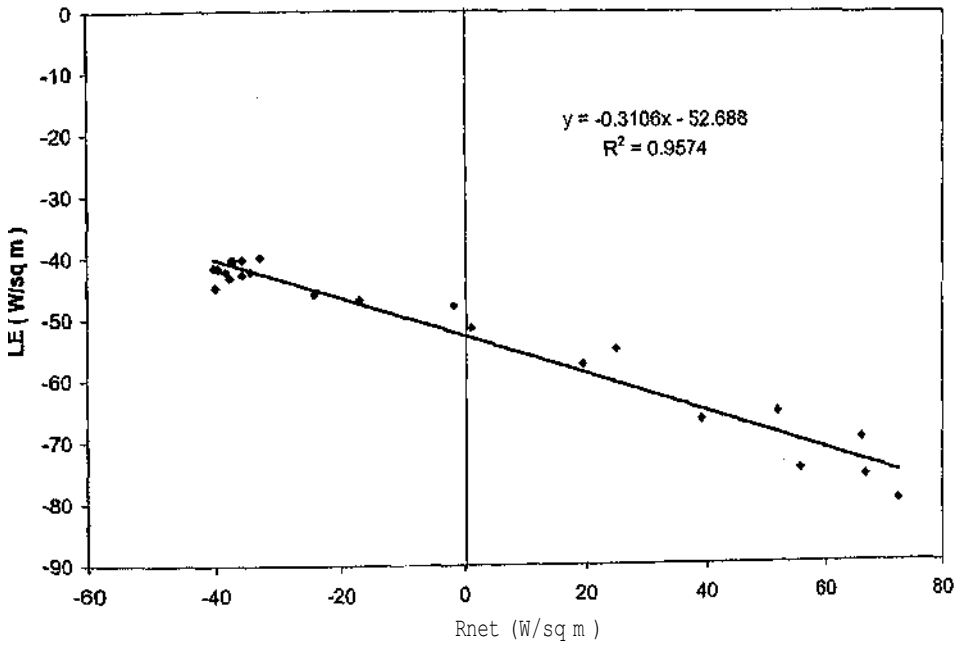

Figure 9: The relationship between net radiation and estimated latent heat flux (Sublimation) based on average diurnal values for March 1999

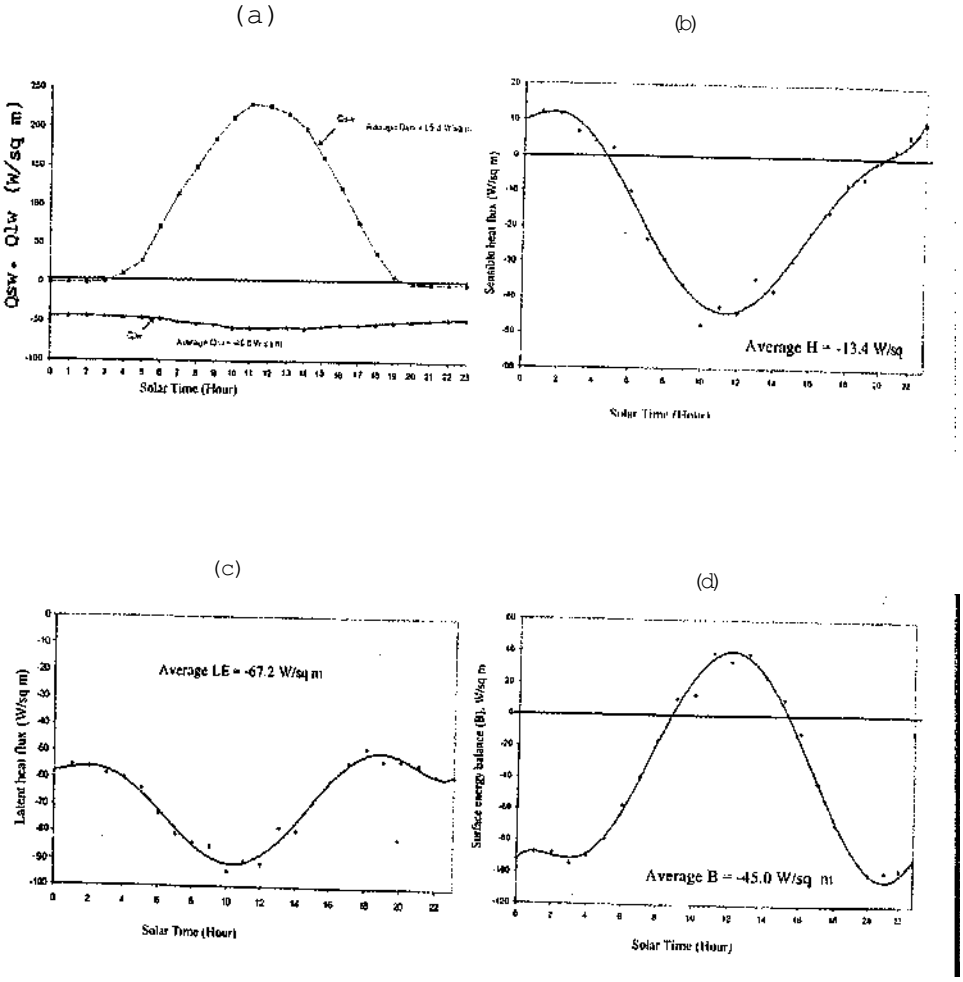

Figure 10 - Mean daily cycle of ice cap surface energy balance components (a) Net short w and net long wave, (b) Sensible heat flux, (c) Latent heat flux and (d)Net surface energy for the month of Feb 1999